Chapter 5

Controlled field evaluation on concrete bridge deck slab using NDT techniques

5.1. Introduction

Among the entire transportation network, bridges are the critical nodes. Recent years have witnessed many cases of a sudden collapse of bridges, possibly due to lack of proper inspection and the use of substandard construction materials (BBC, 2016; HT, 2017; PTI, 2018). Ministry of Road Transport and Highways (MoRTH) has performed a safety audit of 1.6 lakh bridges and has found that more than one hundred structures are in unsound condition and require immediate attention (TOI, 2017). Thus, entire highway infrastructure, including bridges necessitates its timely performance monitoring, in order to avert mishaps and ensure the safety of the citizens.

Bridge deck is one of the major components of the bridge superstructure. It is highly prone to rapid deterioration and has a lesser service life than any other bridge components since it carries moving traffic (Azizinamini et al., 2014). Corrosion of reinforcement is the leading cause of structural deficiency in concrete bridges (Sohanghpurwala, 2006). The other most common deterioration phenomenon observed in bridge decks include deck delamination, vertical cracking and concrete degradation (Gucunski et al., 2013). Corrosion causes expansion of reinforcing steel that generally start cracking which further progresses to fracture planes causing delamination. The separation of concrete in fracture planes from rebar is known as delamination, which is typically a consequence of tensile failure (Sohanghpurwala, 2006). Delamination ultimately leads to open spalls. A delaminated area of 5-20% of the total deck area requires prompt action (Guthrie & Hema, 2005). Factors which cause cracking include traffic loading, ambient temperature changes, and plastic shrinkage. Concrete degradation is due to a reduction in its strength which may be as a result of macro or micro-cracking, effect of freeze-thaw, etc. A substantial amount of money is spent on maintenance and repair of the deck. Due to large dependency of modern society on transportation

systems, efficient assessment of subsurface conditions of bridge decks becomes imperative to extend their service life and reduce the costs incurred in repair (Akgul, 2020).

The most prevalent practice to examine the present state of bridge deck condition is through the visual survey. A subjective opinion could also be provided based on sounding or chain drag operations, when a sharp ringing sound indicates intact concrete, whereas a dull or hollow sound represents the delaminated areas (Oh et al., 2012). Destructive method of coring, do provide some reliable information. Nevertheless, none of these methods has been found to be trustworthy and quick in providing information. A visual survey would provide evidence only when the internal defect has sufficiently progressed up to the surface and becomes visible through naked eyes. Subjective judgement is limited to the experience of professional inspectors and the conditions prevailing during the examination. Cores do not ensure that the condition of the remaining part of the structure is similar, also it is time-consuming, cannot be performed everywhere, and only a limited number of cores can be extracted. Moreover, these inspection and monitoring procedures interrupt traffic by lane closures. This calls for a need to overcome conventional slow and less effective condition assessment and performance monitoring measures.

As demonstrated in the previous chapter, the superiority of Non-Destructive Testing (NDT) is already established to offer a rapid and reliable condition evaluation system for ageing and deteriorating infrastructure by diagnosing problems at an early stage. A number of NDT technologies are found in the literature that have the potential to detect bridge deck deterioration. According to the availability of equipment, Infrared Thermography (IRT) is used in this study along with Ground-Penetrating Radar (GPR). The tests are performed on a fabricated concrete bridge deck slab with simulated defects, and its construction details are presented in Chapter 3. The fabricated slab facilitates conducting the tests and assess their accuracy and precision for defect detection under controlled conditions.

5.2. Evaluation of concrete bridge deck slab using IRT

IRT has been used successfully since the past few decades for detecting concrete subsurface deteriorations including concrete disintegration, cracks, delaminations and voids in roadways or

bridge structures. The internal defects are identified by reading the temperature gradient or thermal contrast (Δt) between the sound and damaged areas as given in Eq. (5.1).

$$\Delta t = t_d - t_s \tag{5.1}$$

where, t_d is the temperature of the damaged area, and t_s is the temperature of the sound area. Theoretically, Δt is mostly positive during day, the delaminated area appears as hot spot, and this time zone is known as day-time heating cycle. During night-time cooling cycle, Δt is negative and the delaminated area appears as cool spot. The technology has advanced to inspect bridge decks by a vehicle travelling at normal driving speed. As stated in earlier chapters, under natural conditions, for passive thermography approach that uses sunlight to heat up the deck slab, the data collection time is a crucial parameter, and active thermography approach using artificial heating sources is not an economical alternative. This is because of the fact that detectability of subsurface flaws requires a minimum temperature difference of 0.5 °C between delaminated and sound areas which varies with time of the day (ASTM D4788-03, 2013). Therefore, several recommendations have been found in the literature about the best time for collecting data through thermographic inspections.

This section discusses the details of the IRT test conducted on the fabricated bridge deck slab simulated with four types of internal defects, namely, delaminations, voids, vertical cracks and corrosion of rebars. However, thermographic inspections failed to provide reasonable results for voids, vertical cracks and corrosion. Therefore, the results of only delamination detection are discussed here. Data was collected manually on the deck slab, every hour over a period of fifteen days in accordance with ASTM standards (ASTM D4788-03, 2013). The thermal camera was hand-held at a height of approximately 1.5 m during data collection. The study intends to explore the following aspects on damage detection using IRT: (a) suitable data collection time; (b) lateral dimensions and thickness of defect; (c) depth of defect; (d) data analysis approach. The impact of camera specifications on IRT results could not be assessed due to the unavailability of any other thermal camera. It should be noted that the theoretical background, instrument details, and imaging basics of IRT are already covered in Chapters 2 and 4, and are not included here to avoid their

repetition. The effect of various parameters on delamination detectability is discussed in the succeeding paragraphs.

5.2.1. Effect of data collection time of the day

To investigate the effect of time of inspection on the detectability of delamination, tests were conducted every hour of the day for a period of two weeks in summer season. The deck slab was fabricated at such a place so that during most of the day-time, sunlight can cover the entire area of the deck. Due to the fact that images were taken manually, the frequency of data collection could not be increased to more than once every hour. In the winter season, extreme cold and cloud cover caused no heating of slab; as a result, the tests conducted during this time failed to produce any reasonable results. Thus, the passive approach of thermography is concluded to be effective when the sunlight is present for a significant duration to heat the area to be inspected. Due to brevity reasons, results of a typical sunny summer day are presented when the ambient temperature ranged between 28-40 °C. Similar results were obtained on all other days of testing.

Thermographic inspections were observed to be more successful during the period of maximum heating in a day, between 10:00 am to 3:00 pm. This is because during the period of sunshine, area above the delaminations heats up faster than the surroundings and the resulting thermal contrast between the sound and delaminated part gets large enough to be detected by thermal imaging cameras. During this time window also, the best results were obtained from 11:00 am to 1:00 pm. A total of seventeen delaminations out of twenty were detectable either fully or partially during this phase. However, as time got nearer to 3:00 pm, most of the delaminations showed a weak response, and after 3:00 pm, there was a drastic drop in their visibility. Only one delamination could be detected with clarity during the tests conducted at the night-time. It showed the effect of temperature inversion, i.e., the delaminated part appeared as cool spot in thermogram, as shown in Figure 5.1. Due to the shallow depth and large dimension of this delamination, cooling cycle effect could be captured using the thermal camera. No other delamination was accurately detectable during night-time. This is because during the cooling phase of the day (after sunset), the temperature of entire slab starts dropping and thermal contrast between the delaminated area and surrounding concrete lowers that makes the detection of delamination difficult through thermal

camera. The deeper the defect, the tougher its detection. These findings were consistent with other research outcomes (Manning & Holt, 1980; Yehia et al., 2007).

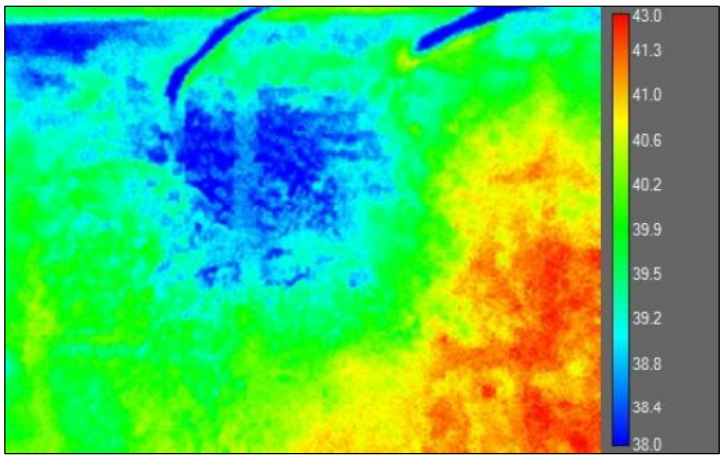

Figure 5.1. Delamination occurring as cool spot in raw thermal image during night-time cooling cycle

Figures 5.2 and 5.3 show the raw thermal images of fully, and partially detectable delaminations, respectively, captured during 11:00 am to 1:00 pm. During this time period, ten delaminations were detected fully, whereas seven delaminations were detected partially. The partial detectability of delaminations could be contributed to the other critical factors, such as lateral dimensions, and depth of placement, as described in section 5.2.2 and 5.2.3. It is noteworthy that the abrupt colour contrast along right side of Figure 5.2 (d) is due to the edge effect and ignored from the judgement. The favourable time window for delamination detection in our study was concluded to be approximately four to five hours after sunrise (10:00 am to 3:00 pm).

5.2.2. Effect of lateral dimensions and thickness of delamination

Theoretically, delaminations with large lateral dimensions would result in larger temperature difference and therefore, the probability of their detection would be higher than the delaminations with small lateral dimensions. In order to study this effect, square-shaped delaminations of four different lateral dimensions were chosen: 5 cm, 10 cm, 15 cm, and 20 cm. Thermography was found to be poor in detecting the 5 cm long delaminations; but quite successful for larger sized delaminations, as seen from Figures 5.2 to 5.4 and Table 5.1. Out of six delaminations of 5 cm

size, only one namely, DL-2/5/B was fully detectable, three delaminations (DL-1/5/A, DL-2/5/A, DL-1/5/B) were partially detectable and two delaminations (DL-1/5/C, DL-2/5/C) were not detectable at all. On the contrary, among four delaminations of 20 cm size, three delaminations (DL-1/20/B, DL-2/20/B, DL-2/20/C) were fully detectable and one delamination (DL-1/20/C) was partially detectable. It should be noted that the actual shape of delaminations was square but they appeared as irregular shaped hot spots in thermograms. This is due to the fact that, in actual field conditions, the temperature variation cannot be linear or abrupt; and the temperature has a gradient within the delaminated as well as the sound concrete area. Estimation of dimensions of the delaminations is therefore, not possible from these images.

Delaminations that were 1 mm and 2 mm thick were simulated in accordance with the actual thickness of delamination which occurs in real field conditions. It is postulated that thicker delaminations would have more probability of detection. Only two sets of such delaminations namely DL-1/5/B and DL-2/5/B; and DL-1/20/C and DL-2/20/C were observed to be consistent with this fact where 1 mm thick delamination was partially detectable whereas 2 mm thick delamination was fully detectable. However, the remaining results of the tests were found to be inconsistent. The detectability of delaminations of both thicknesses having same lateral dimensions and placed at the same depth was found to be quiet similar, such as DL-1/5/A and DL-2/5/A; DL-1/10/C and DL-2/10/C; DL-1/5/C and DL-2/5/C obtained similar outcomes. An exception to both the above findings was DL-1/15/C and DL-2/15/C in which 1 mm thick delamination was partially detectable whereas 2 mm thick delamination was not detectable at all. The possible reason may be attributed to the displacement of the foam pieces during construction process causing error during measurements. It is expected that more difference in thickness may yield substantial effect in thermograms.

5.2.3. Effect of the depth of delamination

In bridge decks, delaminations, generally, occur at the level of reinforcement. Therefore, to scrutinize the impact of delamination depth on its detectability, the simulated delaminations were placed at the level of both reinforcement mats (approximately 40 mm and 136 mm deep). Another condition was created by placing delaminations at 25 mm depth, resulting in three depths of placement.

As anticipated, the detection of temperature differences between sound concrete and delaminations that were placed deep inside the slab was tough. Deep delaminations showed very low temperature variation even during the favourable time window, and therefore, a weak response in thermograms was obtained, as seen from Figures 5.3 and 5.4. Accordingly, most of the delaminations placed at the approximate depth of 136 mm were either partially detectable or not detectable, except DL-2/20/C, which was detectable mostly due to its large lateral dimensions and higher thickness. All three delaminations (DL-1/5/C, DL-2/5/C, DL-2/15/C), which could not be detected were placed at the lowest level (136 mm deep). Delaminations placed at an intermediate depth of 40 mm were fully detectable, except DL-1/5/B, which was partially detectable. Shallow delaminations (placed at 25 mm depth) were either fully or partially detectable, depending on their lateral dimensions. Delaminations of 5 cm size namely, DL-1/5/A and DL-2/5/A, placed at 25 mm depth, were partially detected since due to their small size, the generated thermal contrast was very less to be clearly detected. The effect of large lateral dimensions was found to be valid in this case as well, in view of detectability of 10 cm square delaminations at 25 mm depth (DL-1/10/A, DL-2/10/A) (refer Figure 5.2). It is, however, not possible to estimate the depth of delamination from the thermograms. Further, coring at those locations or other precise NDT method would be required to determine the depth of the defect. In addition to this, better quality thermal cameras may enable better determination of deeper defects.

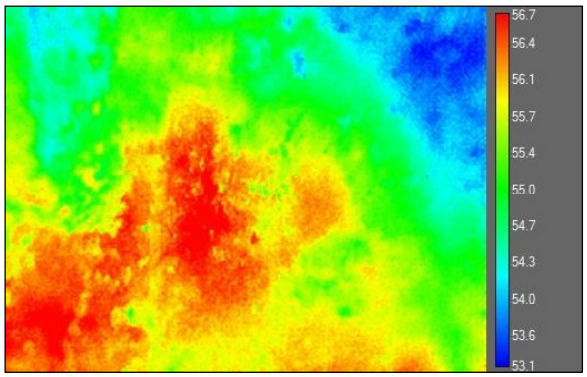

(a) DL-1/10/A

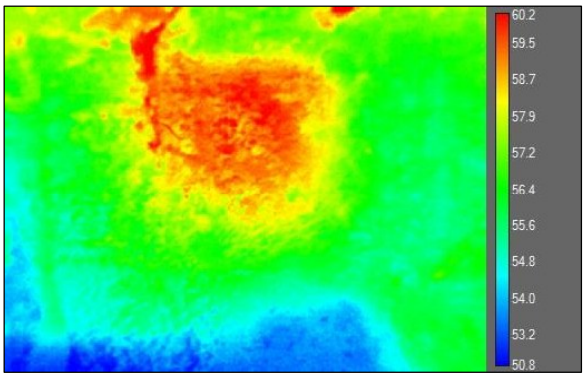

(b) DL-2/10/A

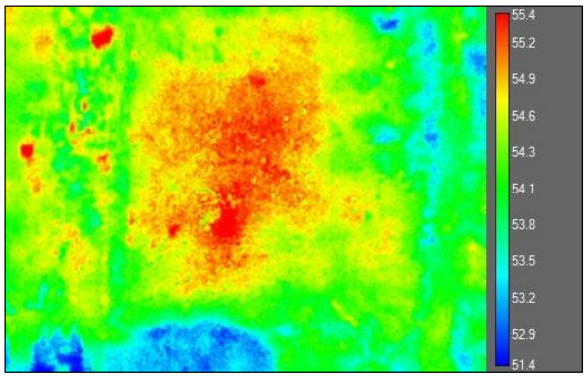

(c) DL-1/15/B

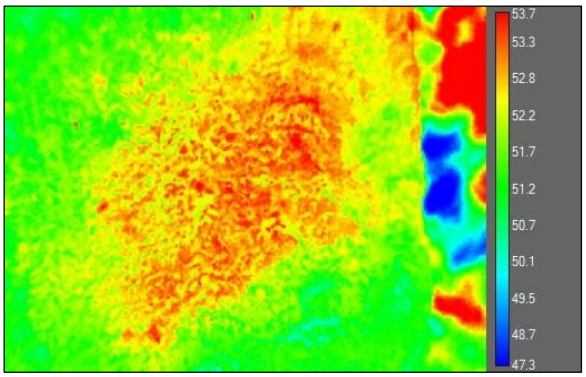

(d) DL-2/15/B

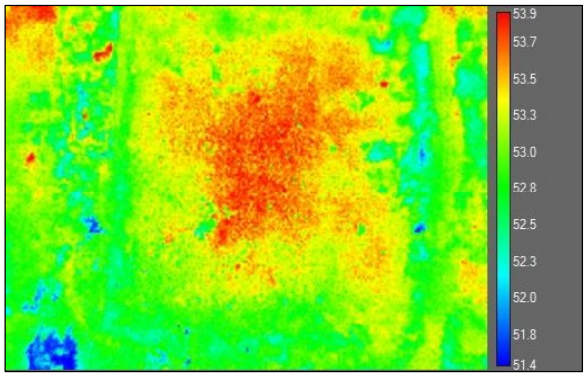

(e) DL-1/10/B

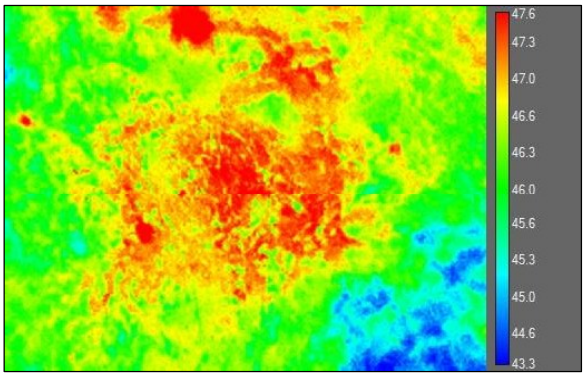

(f) DL-2/5/B

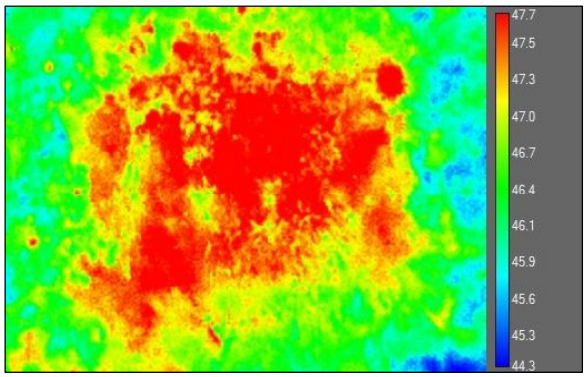

(g) DL-1/20/B

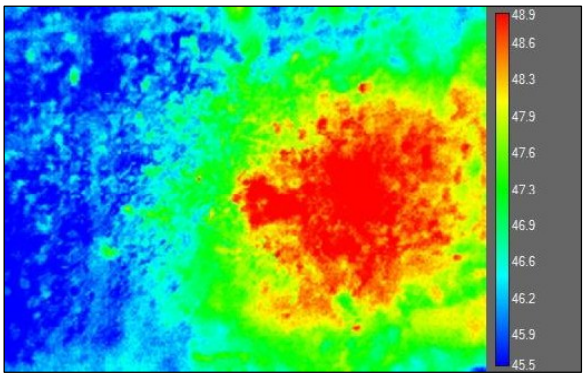

(h) DL-2/20/B

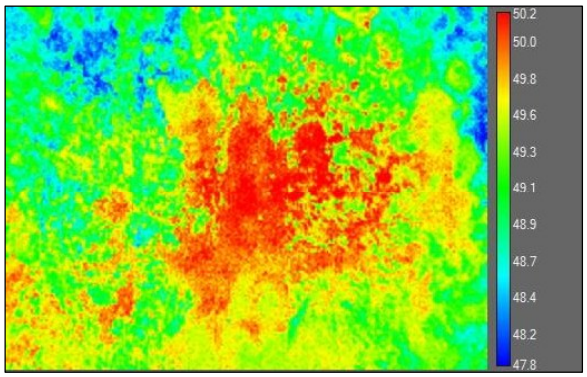

(i) DL-2/10/B

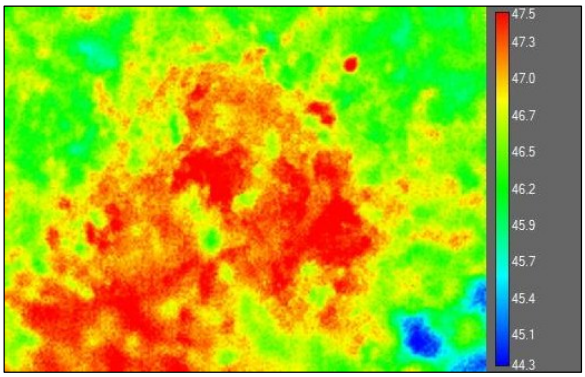

(j) DL-2/20/C

Figure 5.2. Raw thermal images showing fully detectable delaminations as hot spots taken during 11:00 am to 1:00 pm

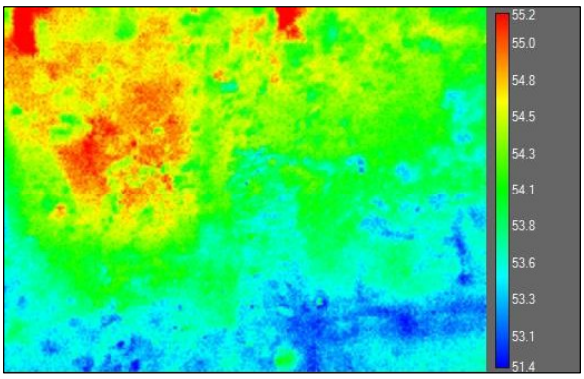

(a) DL-1/5/A

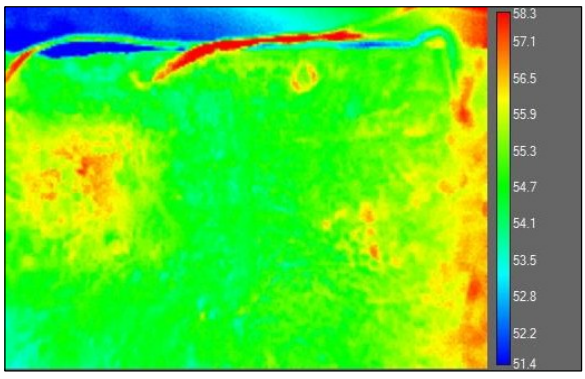

(b) DL-2/5/A

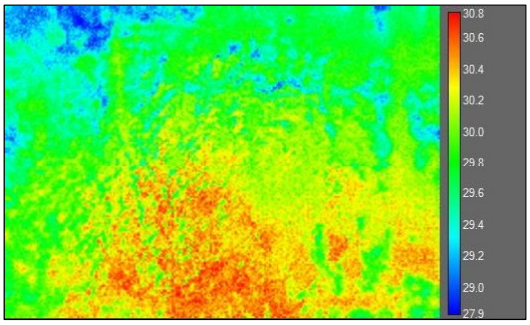

(c) DL-1/10/C

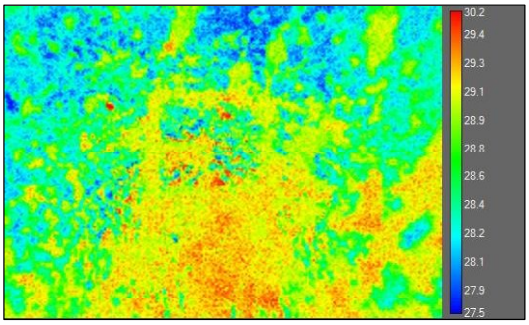

(d) DL-2/10/C

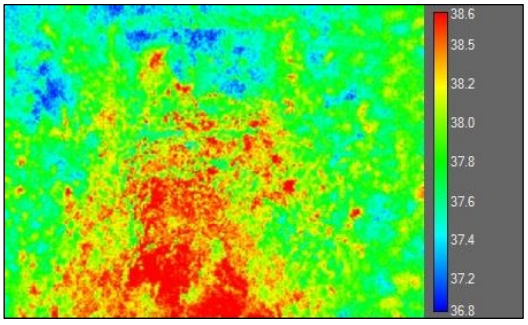

(e) DL-1/20/C

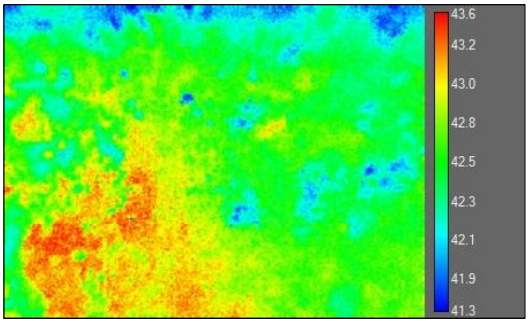

(f) DL-1/5/B

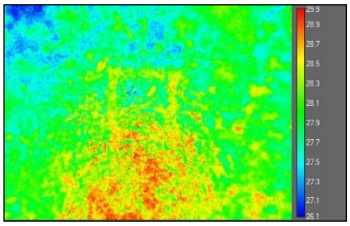

(g) DL-1/15/C

Figure 5.3. Raw thermal images showing partially detectable delaminations as hot spots taken during 11:00 am to 1:00 pm

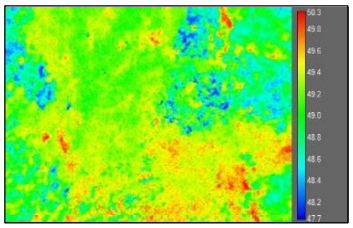

(a) DL-1/5/C

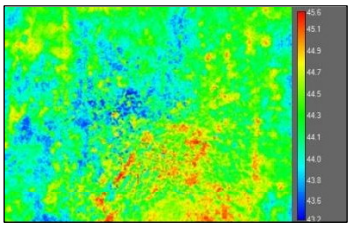

(b) DL-2/5/C

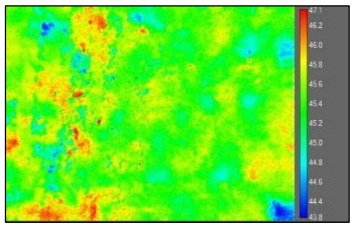

(c) DL-2/15/C

Figure 5.4. Raw thermal images of undetectable delaminations

5.2.4. Data analysis approach

As discussed earlier, delaminations are visible in the thermal images during the favourable time window of the day. However, sometimes it is not possible to detect these defects just by observing colour variations in raw IR images. The unclear colour contrast in images would lead to different subjective judgements by different persons. This is because of the presence of too much noise in the image, which requires further processing. The deck slab itself undergoes a temperature gradient depending on position and orientation of the sun and adds to this noise. Therefore, an objective approach using MATLAB has been explored in this study. The processing using MATLAB facilitated the clearance of the noise to an appreciable extent. As a result, visibility of delaminations enhanced in the images which earlier showed a weak response. Nevertheless, for the images that showed no response to any delamination, such as those taken during the night-time, the processing also could not contribute to produce the desired outcome. Hence, this approach of processing has been adopted in this study to improve and ease the visibility of delamination in thermograms, in which the noise obscured the response of the delamination.

The objective of the MATLAB analysis was to distinguish the delaminated area in the thermogram. It is already known that every thermal image contains a temperature scale representing the minimum and maximum value of temperature in that image. Therefore, for the purpose of this analysis, the numeric value associated with each pixel in this temperature scale was used. The range of 0 to 255 pixels in grayscale range was converted into binary form of 0 (“black” in MATLAB) and 1 (“white” in MATLAB). In our study, delaminated areas were at higher temperatures than the sound areas, and were marked as hot spots. Practically, the surface temperature of the sound, as well as the delaminated area, cannot become homogeneous throughout. The variation in both cases is within a range of temperatures. However, it is difficult to quantify this variation into a binary form of 0 and 1. To ease this, since the delaminated area is hotter than the surrounding sound area, it was assumed that all the temperature values higher than the lowest temperature of delaminated part are constant, and represent delaminated area. Therefore, all the pixel values corresponding to the temperatures between the lowest temperature of delaminated part and the maximum temperature in the thermal image are assigned the value as 0 (black). All the temperature values lower than the lowest temperature of delaminated part are

assumed to be constant and represent sound area. Therefore, all the pixels corresponding to the range of temperatures between the lowest temperature of delaminated part and minimum temperature of the image are assigned the value as 1 (white). This can be mathematically written as follows:

$T(x, y)$ is the pixel value of any temperature, T_{del} is the lowest temperature of delaminated area, and T_{max} and T_{min} represent the maximum and minimum temperature in the thermal image, respectively. Then, according to Eq. (5.2):

$$F(x,y) = \begin{cases} 0, & if\ T_{del} \leq T(x,y) \leq T_{max} \\ 1, & if\ T_{min} \leq T(x,y) < T_{del} \end{cases} \tag{5.2}$$

where, $F(x, y)$ is the value of each element of binarized image.

This procedure is a more objective way to assess a delaminated area which is displayed as black while sound area is shown as white, rather than examining the raw thermal images. The partially detected delaminations presented in Figure 5.3 are processed in MATLAB. The resulting images which are presented in Figure 5.5 show their enhanced clarity and ease of understanding due to the removal of background noise. The images indicate delamination in the form of an irregular shaped black colour area. The black colour area is not closely packed, possibly due to the variation in temperature within the delaminated area as well, and non-uniform heating through the passive source (sunlight). Further future research may be undertaken to take into account the temperature variations as well, and accordingly, the proposed approach can be improved further.

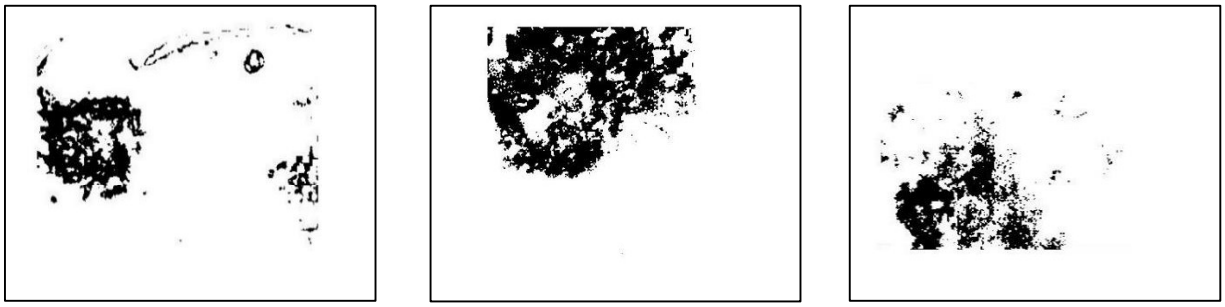

(a) DL-2/5/A **(b) DL-1/5/A** **(c) DL-1/5/B**

(d) DL-1/10/C **(e) DL-2/10/C** **(f) DL-1/15/C**

(g) DL-1/20/C

Figure 5.5. Processed thermal images of partially detectable delaminations

5.3. Evaluation of concrete bridge deck slab using GPR

Following the recommendations made by the researchers that highlight the superiority of using a combination of NDT methods rather than merely relying on estimates from a single method, applications of GPR are explored on bridge deck slab in addition to IRT. Improvements in extracting knowledge about defects owing to the use of another method, if any, are noted.

Applications of GPR in bridge decks include concrete mapping, detection of voids, honeycombing, delamination, rebar depth, and moisture content (Yehia et al., 2007). Many interpretations have been mentioned in the literature for the detection of subsurface defects in concrete bridge decks through the GPR data. Any changes in the reflection strength,

In general, continuous hyperbolic reflections of uniformly high magnitude with relatively short arrival times are characterized by areas of sound concrete with reinforcement mat. On the other hand, dull reflections with low amplitude, discontinuous hyperbolas, extra peaks, or apparent change in position of reinforcement indicating a change in arrival times due to difference in material, specifies signs of deterioration, and abnormality. Figure 5.6 shows the delamination DL-1/20/B (encircled) appearing over the top rebars with dull reflection, approximately at a distance of 100 cm from the slab end, as verified from the drawing. The bright hyperbolic reflections are obtained from the upper rebars of top reinforcement mat and the peak of the hyperbolas indicates the apex of these bars. Figure 5.7 shows the reflection of DL-2/10/A, appearing as an extra peak with low intensity of brightness than the normal rebars. Similarly, Figure 5.8 shows the reflection of DL-2/20/B.

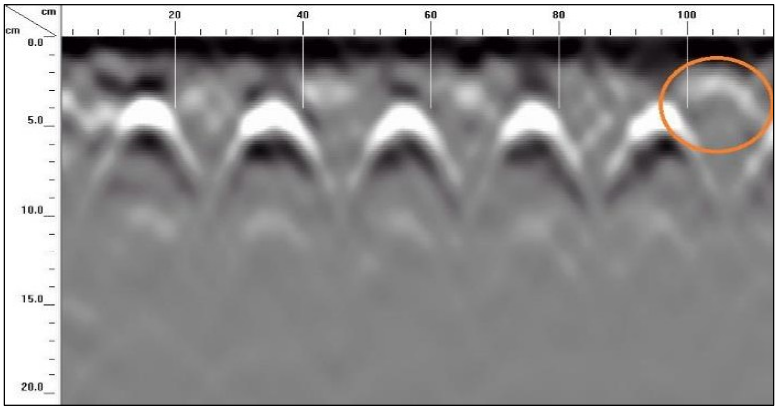

Figure 5.6. Sectional profile showing reflection of DL-1/20/B

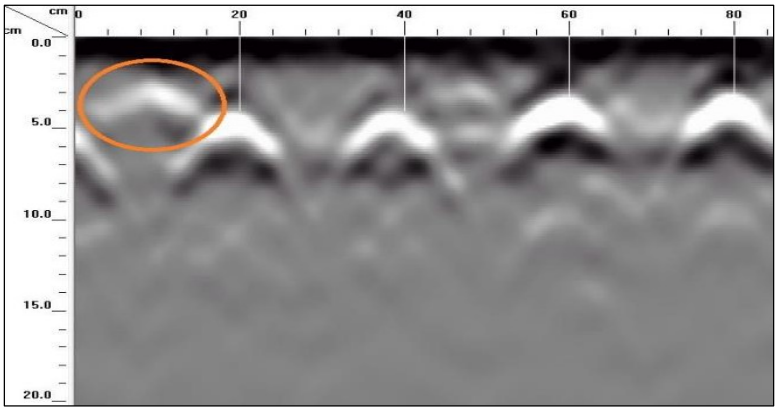

Figure 5.7. Sectional profile showing reflection of DL-2/10/A

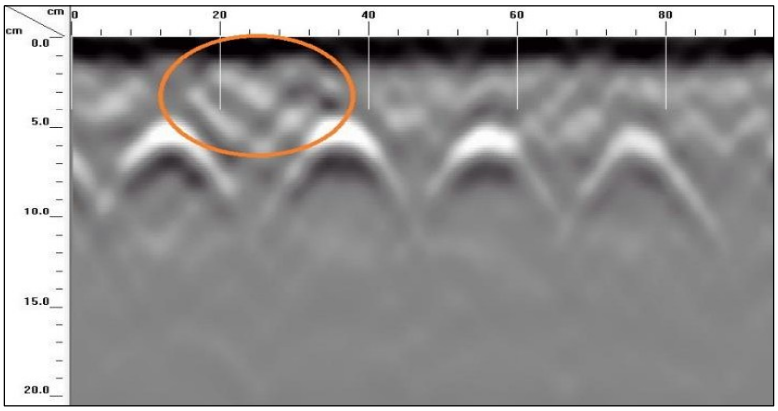

Figure 5.8. Sectional profile showing reflection of DL-2/20/B

Figures 5.9 and 5.10 present the voids V_1 and V_2 in the GPR linescans.

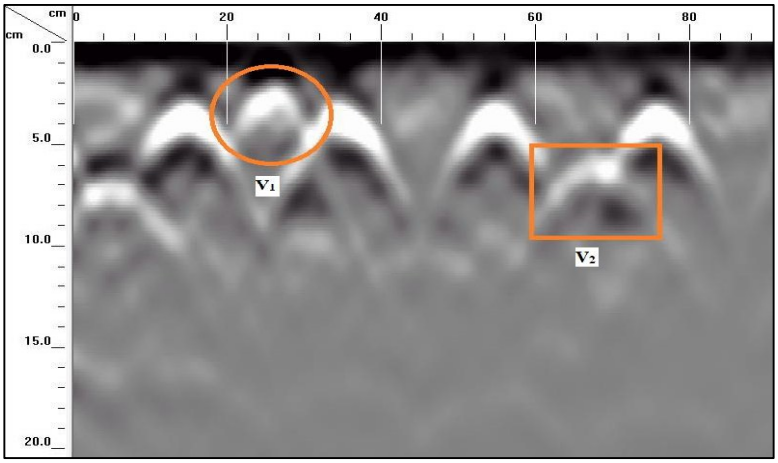

Figure 5.9. Sectional profile showing voids V_1 and V_2

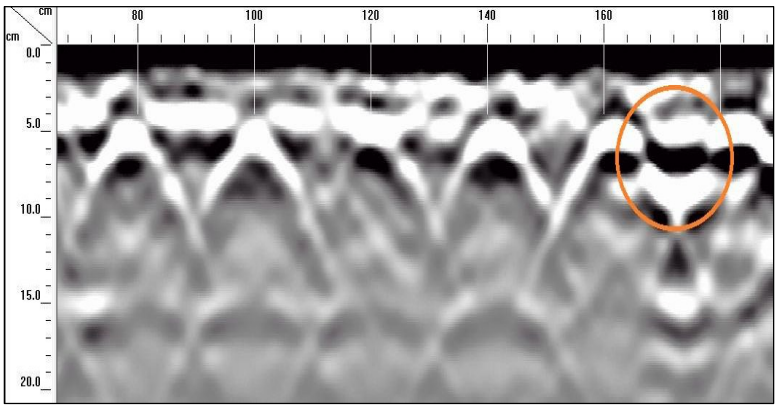

Figure 5.10. Sectional profile showing void V_1

Figure 5.11 shows delaminations DL-1/15/B and DL-2/15/B, as indicated by multiple low amplitude reflections, and rebar reflection in this part appearing at a deeper level than its actual depth possibly due to the reduction in signal velocity caused by delamination.

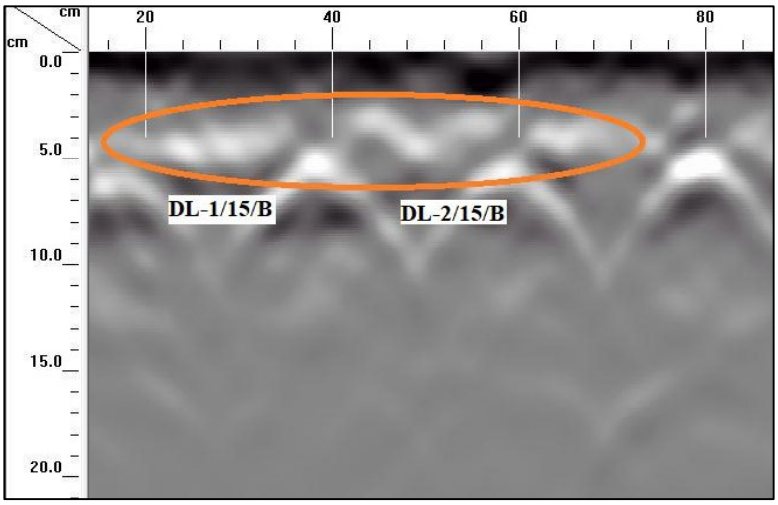

Figure 5.11. Sectional profile indicating DL-1/15/B and DL-2/15/B

Figure 5.12 indicates DL-1/10/B, and DL-2/10/B, identified as discontinuity in reflection of upper rebars. Figure 5.13 shows the upper, and lower rebars in the sectional profile. Their transverse, and longitudinal alignment is clearly seen in the figure.

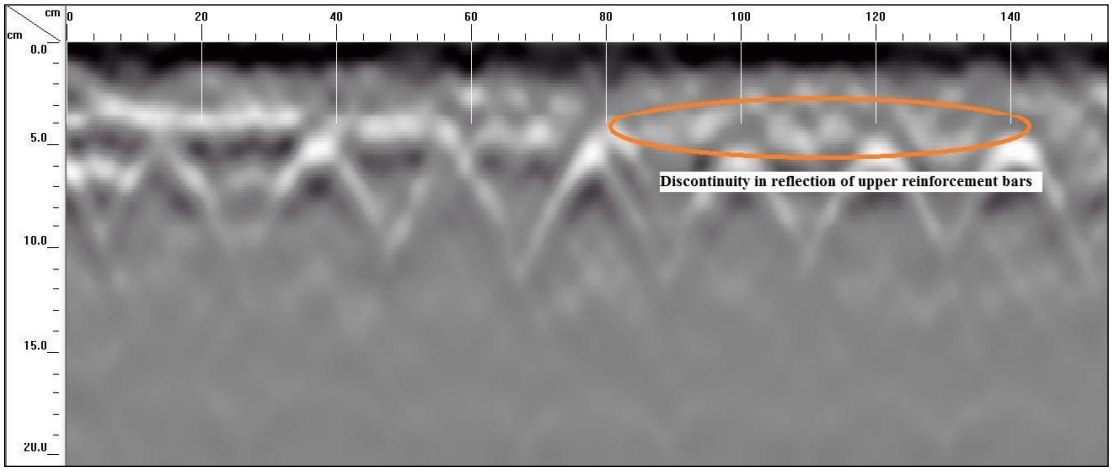

Figure 5.12. Sectional profile indicating DL-1/10/B and DL-2/10/B

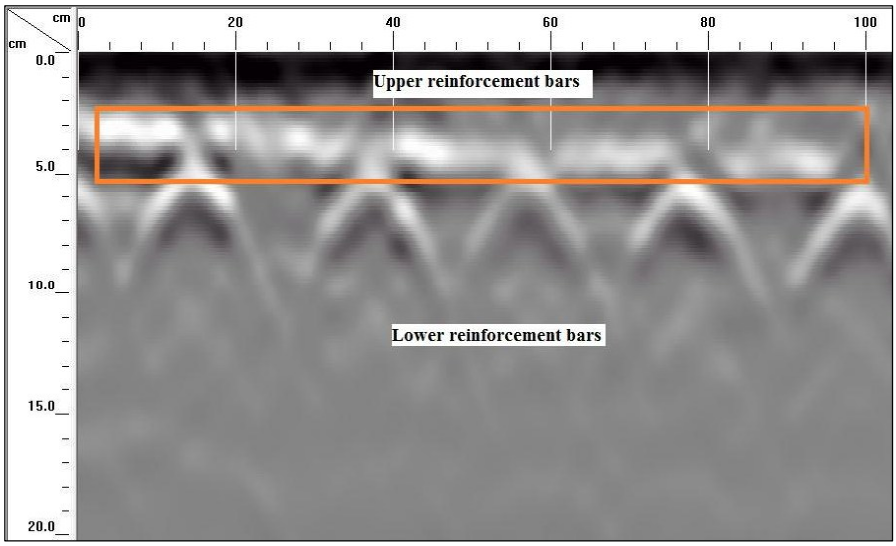

Figure 5.13. Upper and lower rebars of top reinforcement mat

Reflections obtained from rebars are bright and strong. In the process, the other reflections from non-metallic objects often get obscured. It can be seen from the GPR linescans that only seven out of twenty simulated delaminations, and voids could be detected. Among the detected delaminations, those located up to the depth of the top reinforcement mat could produce some reflection in the scans. The prominent reason for inability in detection is because the reflection produced by delaminations or voids in linescans are often dull as compared to the reflections of metal bars. Therefore, when seen in GPR linescans, such objects get obscured due to the presence of metal objects that are rebars in the present case. For the similar reasons, other defects simulated on bottom reinforcement mat could not produce sufficient reflection. The findings are also consistent with those reported in the literature that direct detection of delamination using GPR is difficult unless they contain enough moisture. Presence of water increases the dielectric contrast and ease their visibility.

5.4. Concluding remarks

This chapter presents the results of testing conducted on the fabricated concrete bridge deck slab using IRT and GPR. The detectability of defects through any of these NDT technologies is found to depend upon various factors, such as depth and dimensions of the defect. Several other parameters that are specific to the technology also adversely affect their performance. For example,

time of the day has great impact on success of IRT tests, whereas dielectric contrast between the target and host material govern the detectability through GPR tests. Table 5.1 summarizes the results of delamination detectability obtained through IRT and GPR.

Table 5.1. Performance summary of NDT technologies on fabricated concrete bridge deck slab

Defect code	Detectability using IRT	Detectability using GPR
DL-1/5/A	PD	ND
DL-2/5/A	PD	ND
DL-1/10/A	D	ND
DL-2/10/A	D	D
DL-1/15/B	D	D
DL-2/15/B	D	D
DL-1/15/C	PD	ND
DL-2/15/C	ND	ND
DL-1/5/C	ND	ND
DL-2/5/C	ND	ND
DL-1/5/B	PD	ND
DL-2/5/B	D	ND
DL-1/10/B	D	D
DL-2/10/B	D	D
DL-1/10/C	PD	ND
DL-2/10/C	PD	ND
DL-1/20/B	D	D
DL-2/20/B	D	D
DL-1/20/C	PD	ND
DL-2/20/C	D	ND
V_1	ND	D
V_2	ND	D
VC_1	ND	ND
VC_2	ND	ND
CR	ND	ND

*D: detected; PD: partially detected; ND: not detected

As seen from the results, it can be concluded that IRT performed satisfactorily in identifying shallow and large-sized delaminations. However, the technology has shown poor performance in detecting deep and small-sized delaminations and thus, could be better employed as a near-surface

detection method. Use of a superior quality thermal camera with high resolution may ensure clear detection of partially detectable delaminations and some improvement in detection of small-sized delaminations may be obtained. The developed data analysis approach assisted in removing some noise from the thermal images and offered easier interpretation of the defects. The study concluded 4-5 hours after sunshine as the ideal time for conducting field inspections on concrete bridge decks using IRT. The time of testing should be judiciously monitored otherwise results may lead to wrong interpretations. Misleading judgements in thermograms could also occur due to edge effect. Additionally, it is not possible to determine the exact geometry or depth of the defect using IRT. In the present study under the specified conditions and equipment, the method failed to detect voids, vertical cracks and corrosion. Nevertheless, it is preferred NDT technique owing to ease, rapid data collection even at traffic speed, and covering large areas.

A combination of GPR along with IRT added advantage to extract other details of the defects. Although GPR tests obtained little success in the detection of internal flaws yet they facilitated estimation of the approximate depth of the detected defects and assisted to overcome this limitation of IRT. Voids and a few of the delaminations placed along top reinforcement mat could be vaguely identified through the sectional profiles. This is because most of the reflections from defects got overshadowed by the bright reflections of the rebars. As such, detection of air-filled delaminations is a limitation to GPR method. Presence of moisture is expected to produce distinct reflections, and enhance the chances of delamination and void detection. Corroded mat of reinforcement could not produce distinct reflection, a greater degree of corrosion on bars is expected to produce some peculiar reflections. Vertical cracks being very less in thickness, also could not generate desired results.

It is recommended to use other NDT technologies, such as impact echo, in collaboration with GPR and IRT to ensure the reliability in measurements of defects. An integrated implementation of these three methods can be done in the way that thermography can first scan the entire area and demarcate the defected areas. Further testing on these demarcated areas using GPR would help to ascertain the position and size of defects. Finally, impact echo tests may verify the findings and ensure reliability in estimates. However, due to unavailability of impact echo equipment, it could not be used in the present study.

Briefly, it can be concluded that both the NDT technologies have performed fairly well in detecting subsurface defects, in this study. These are expected to produce better results by adopting the use of superior quality cameras, and further refining the process of their data analysis. An approach for post-processing of thermograms using MATLAB has been developed, and presented in this chapter. Similarly, use of advanced algorithms for GPR data analysis may deliver better identification of defects. However, this in itself is a big task, and beyond the scope of present study. The next chapter discusses the in-field investigations of pavement condition using NDT techniques and forms the basis of the case study to demonstrate the pavement maintenance and repair decision-support approaches.